

Supplementary Materials for

Arginine Starvation Impairs Mitochondrial Respiratory Function in ASS1-Deficient Breast Cancer Cells

Fuming Qiu, Yun-Ru Chen, Xiyong Liu, Cheng-Ying Chu, Li-Juan Shen, Jinghong Xu, Shikha Gaur, Henry Jay Forman, Hang Zhang, Shu Zheng, Yun Yen, Jian Huang, Hsing-Jien Kung, David K. Ann*

*Corresponding author. E-mail: dann@coh.org

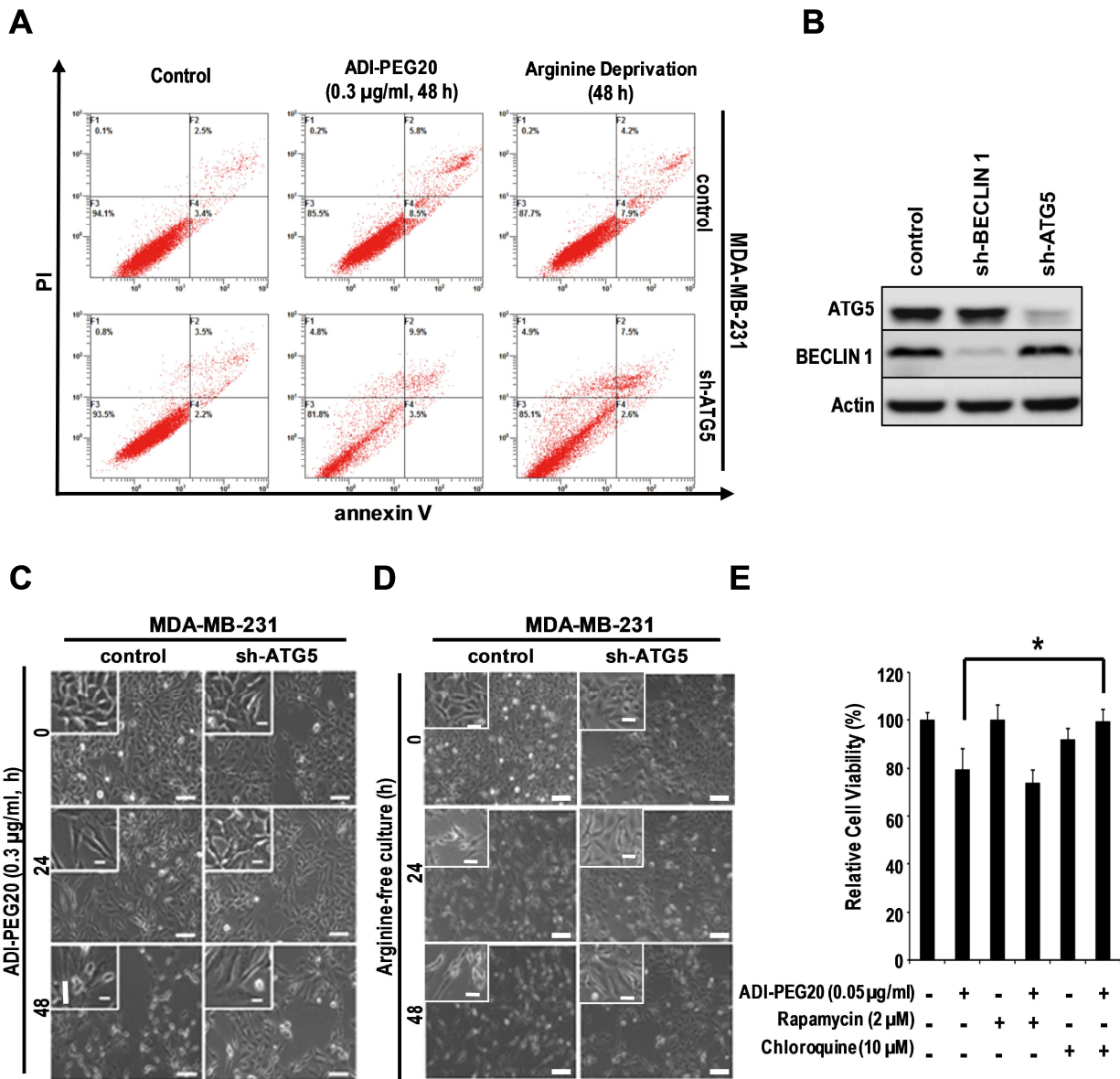
Published 1 April 2014, *Sci. Signal.* 7, ra31 (2014)
DOI: 10.1126/scisignal.2004761

The PDF file includes:

- Fig. S1. Knockdown of ASS1 increases sensitivity to ADI-PEG20 treatment.
- Fig. S2. Autophagy is required for ADI-PEG20-induced cell death.
- Fig. S3. Arginine depletion suppresses the basal oxygen consumption rate and reserve capacity.
- Fig. S4. ADI-PEG20 does not affect *SOD* and *SIRT* mRNA abundance, but decreases mitochondrial protein abundance.
- Fig. S5. ADI-PEG20 causes mitochondrial fragmentation in MDA-MB-231 cells.
- Fig. S6. ASS1 abundance predicts OS.
- Fig. S7. Lack of synergistic effect of ADI-PEG20 combined with Abraxane or carboplatin.
- Table S1. Primer sequences.

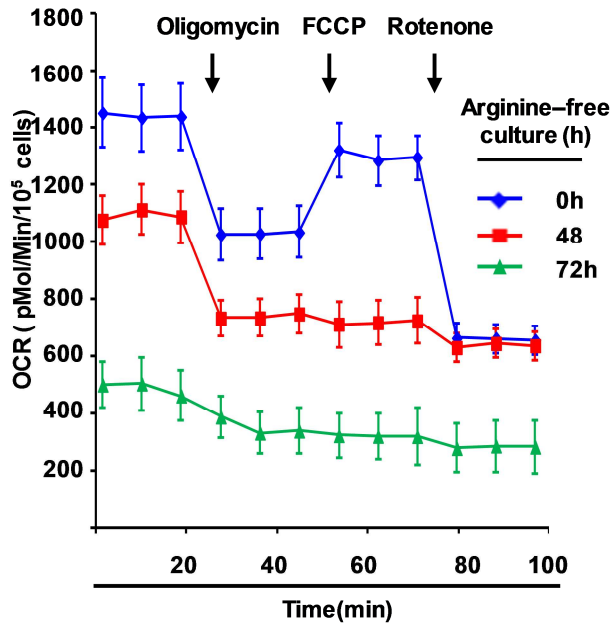
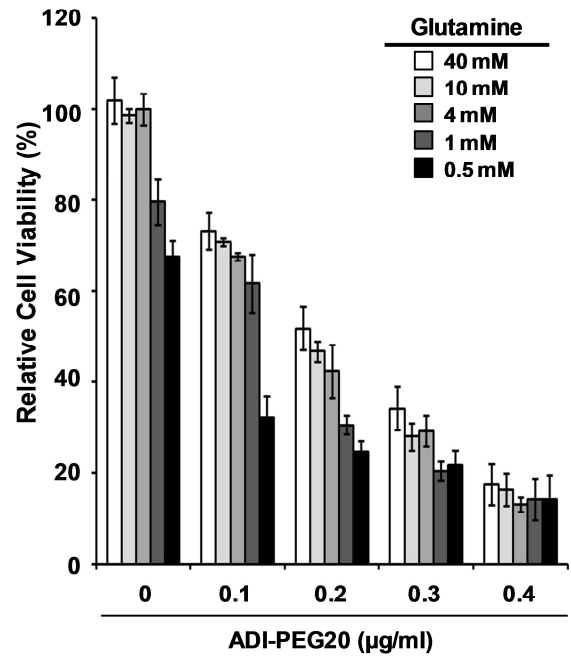
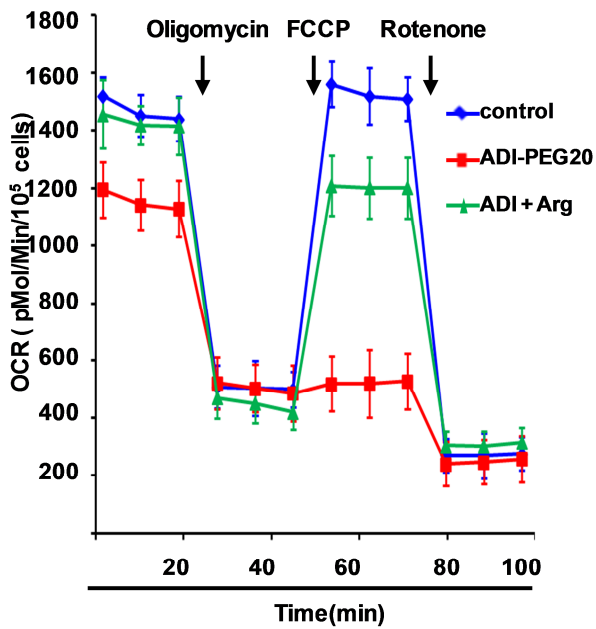
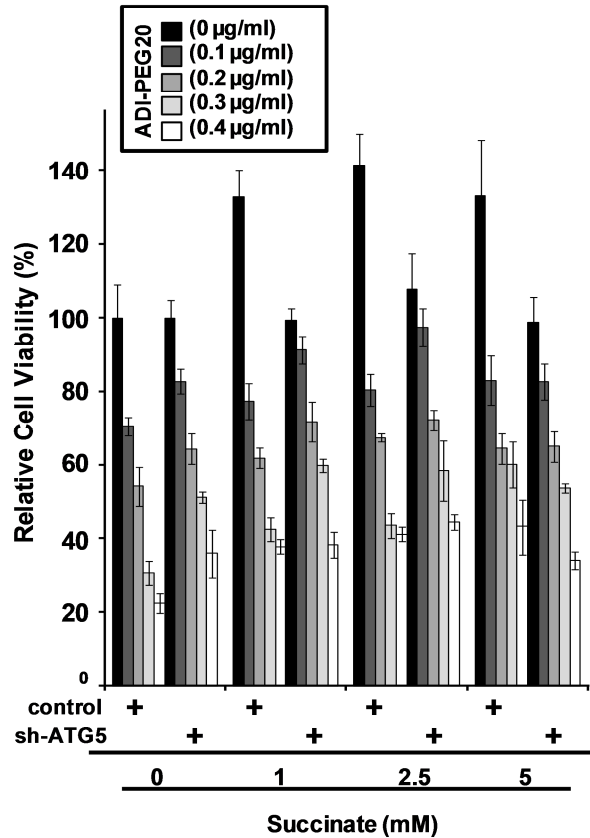
Supplemental Fig. S1. Knockdown of ASS1 increases sensitivity to ADI-PEG20 treatment.

(A) MDA-MB-231 cell proliferation is sensitive to ADI-PEG20 in time course growth assays. The respective cell index at 0 hour treatment is designated as 1; N = 5 sets of cells. (B and C) ASS1-overexpressing MDA-MB-231 (B) and ASS1-knockdown T47D (C) cells were established by lentiviral transduction. The abundance of *ASS1* mRNA and ASS1 protein were confirmed by qRT-PCR and Western analyses, respectively; N = 3 sets of cells. (D and E) Knockdown of ASS1 sensitizes T47D cells to ADI-PEG20 analyzed by time course growth assays (D) and anchorage-independent colony formation (E). The relative cell proliferation in (D) is plotted against the tracing from respective cells at 0 hour treatment; N = 5 sets of cells. (E) Representative images show overall view or a selected area of colony growth (enlarged; *insets*). The number of colonies from three independent experiments were calculated and plotted as bar graph (*right*); N = 3 independent experiments performed in duplicate; *: $p < 0.05$. (F) qRT-PCR and Western analyses of *ASS1* mRNA and ASS1 protein abundances in MCF-7 cells showing a 90% decrease in mRNA abundance, but only 50% decrease in protein abundance. The relative *ASS1* mRNA abundance is calculated as described in Fig. 1A. qRT-PCR data are shown as mean \pm SD; N = 3 sets of cells.



Supplemental Fig. S2. Autophagy is required for ADI-PEG20–induced cell death. (A) ADI-PEG20 treatment (*middle panels*) or arginine starvation (*right panels*) moderately increases apoptotic cell percentage in MDA-MB-231 cells. Knockdown of ATG5 in MDA-MB-231 cells does not significantly affect annexin V/PI profiling in response to ADI-PEG20-treatment or arginine-starvation (*lower panels*). Representative images are shown; N = 5 sets of cells. (B) The reduced abundance of autophagy proteins, ATG5 and BECLIN 1, by knockdown was verified by

Western analyses. (C and D) Autophagy is required for growth inhibition by ADI-PEG20 (C) and arginine-deprivation (D). Representative phase contrast image of arginine-starved MDA-MB-231 cells shows morphological changes that are not seen in ATG5-knockdown MDA-MB-231 cells. Bar: 200 μ m and 50 μ m (zoomed); N = 3 sets of cells. (E) Chloroquine (an autophagy inhibitor), but not rapamycin (an autophagy inducer), affects ADI-PEG20-induced cell death. The relative cell viability showing in percentage is determined by ACP assay and uses the value from 0 μ g/ml treatment as the reference. Results are shown as the mean \pm SD; N = 5 sets of cells; *: $p < 0.05$.

A**B****C****D**

Supplemental Fig. S3. Arginine depletion suppresses the basal oxygen consumption rate and reserve capacity. (A) OCR was normalized using cell numbers and is shown as the mean \pm SD; N = 3 sets of cells. (B) Glutamine supplementation does not rescue the cytotoxic effect induced by ADI-PEG20. Cell viability was determined using the value from cells treated with vehicle (ADI-PEG20 (0 μ g/ml) and glutamine (4 mM)) set as 1. Results are shown as the mean \pm SD; N = 3 sets of cells. (C) Supplementation of arginine rescues OCR in ADI-PEG20-treated cells. OCR was normalized using cell numbers and is shown as the mean \pm SD; N = 3 sets of cells. (D) Succinate reverses the ADI-PEG20-induced growth inhibition. MDA-MB-231 and corresponding ATG5-knockdown cells were treated with the indicated combinations of ADI-PEG20 and succinate. Cell viability was determined by ACP assay using the value from cells treated with vehicle (ADI-PEG20 (0 μ g/ml) and succinate (0 mM)) set as 1. Results are shown as the mean \pm SD; N = 3 sets of cells.

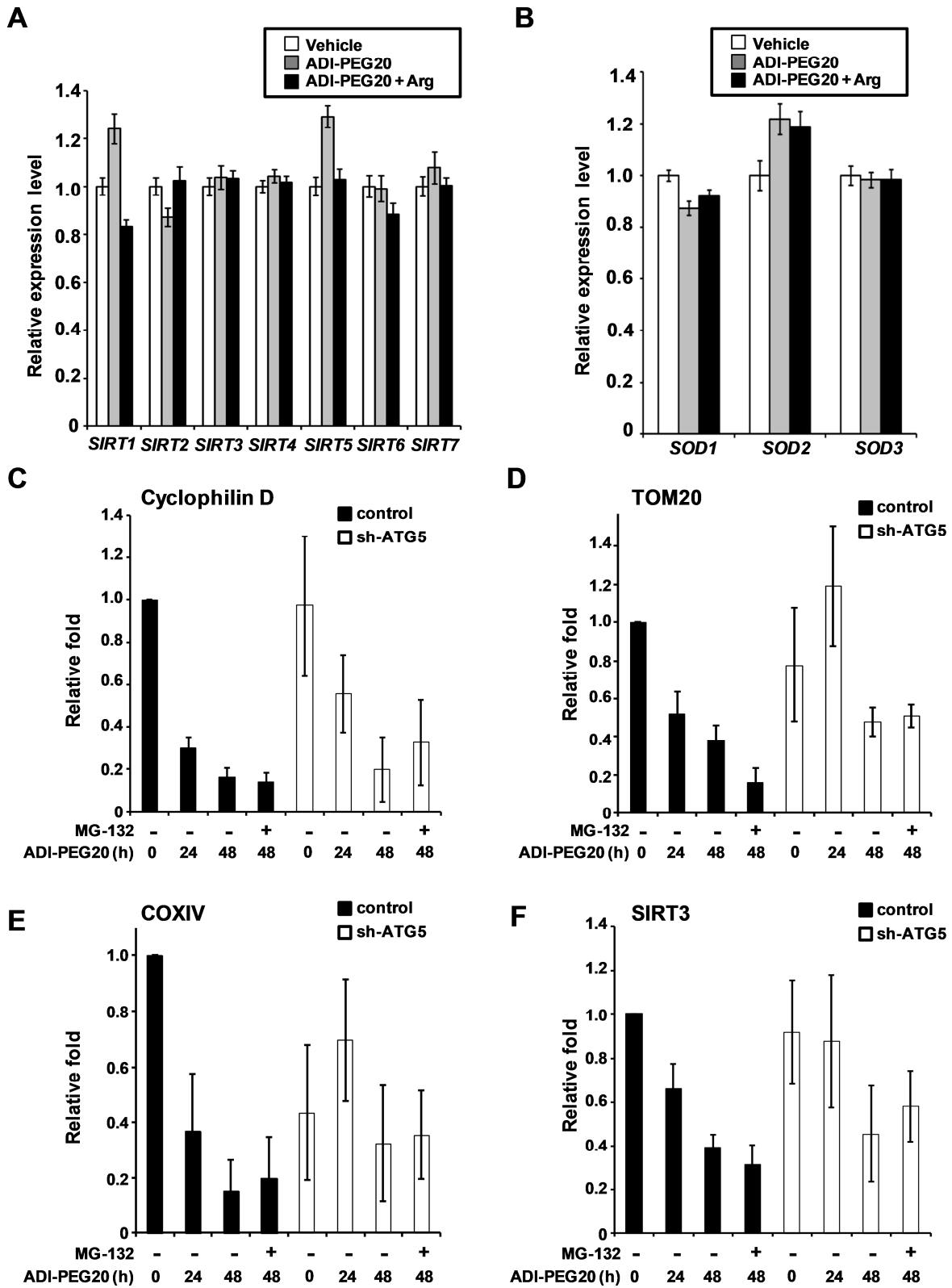
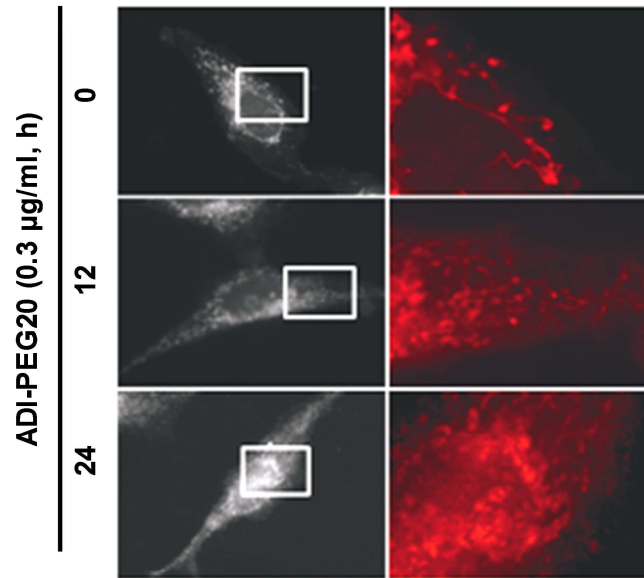


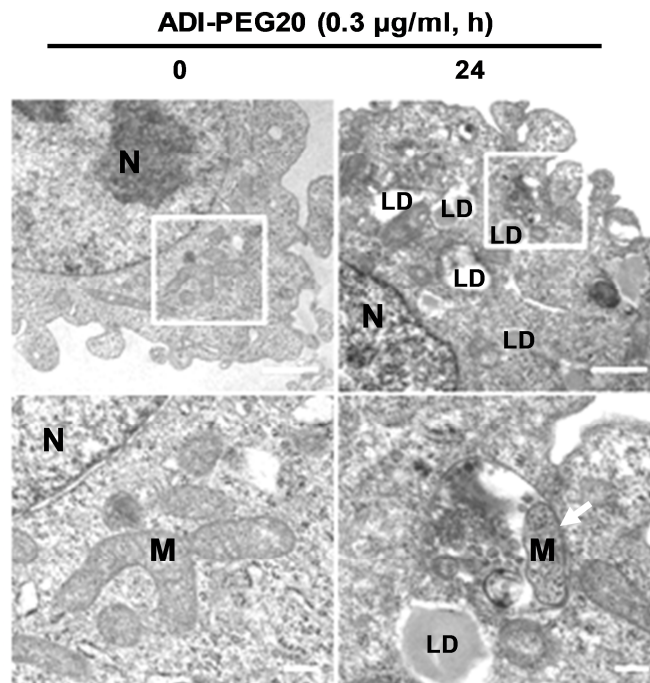
Figure.S4

Supplemental Fig. S4. ADI-PEG20 does not affect *SOD* and *SIRT* mRNA abundance, but decreases mitochondrial protein abundance. (A and B) qRT-PCR analyses validate the relative steady-state abundance of *SIRT* (A) and *SOD* (B) mRNA extracted from array data. The relative abundance of *SIRT3* and *SOD2* mRNA show no differences in response to ADI-PEG20 with or without arginine supplementation rescue. Results are shown as the mean \pm SD; N = 3 sets of cells. (C - F) Bar graph shows the quantitative analysis of densitometric tracing for mitochondrial proteins Cyclophilin D (C), TOM20 (D), COXIV (E) and SIRT3 (F) shown in Fig. 4D after normalization with actin. Results are shown as mean \pm SD; N = 3 sets of paired cells.

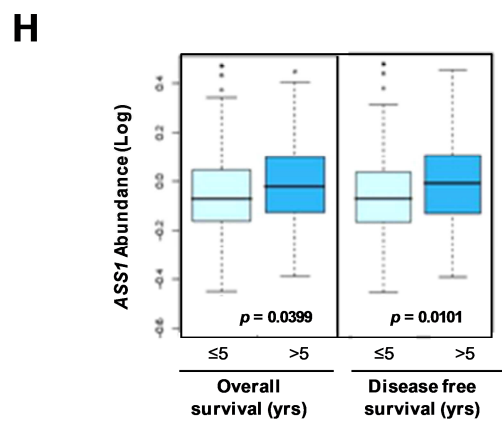
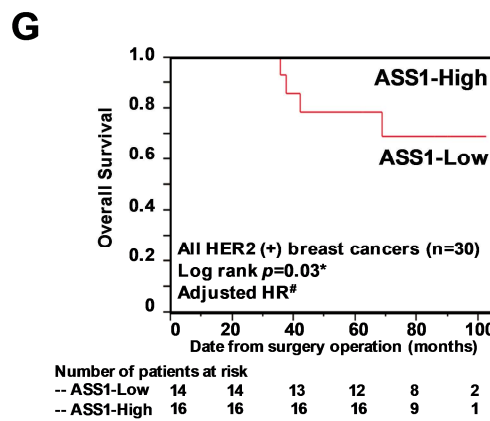
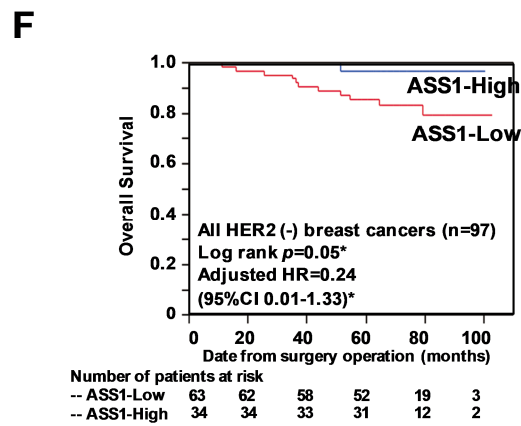
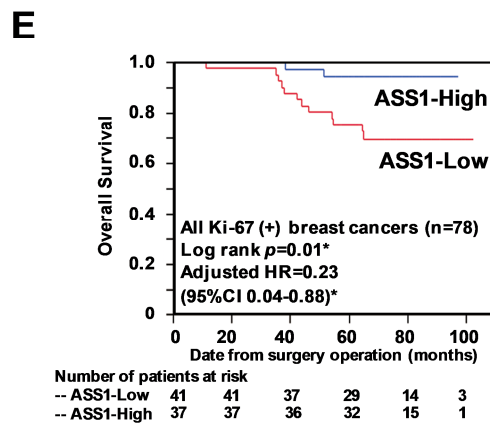
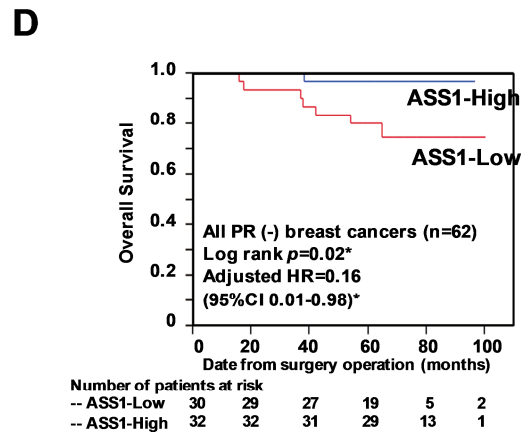
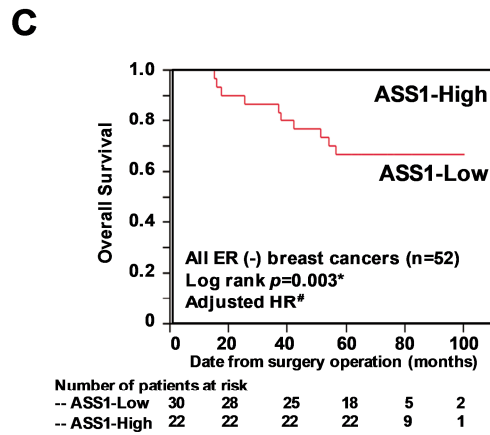
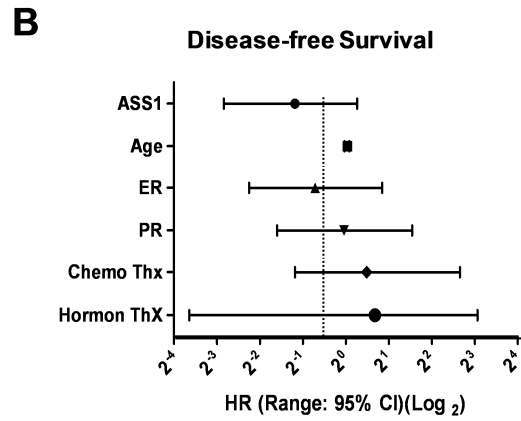
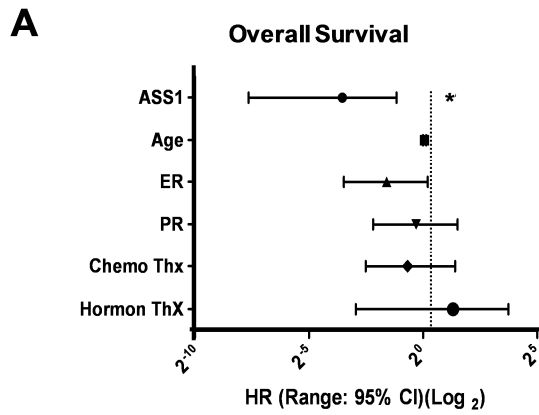
A



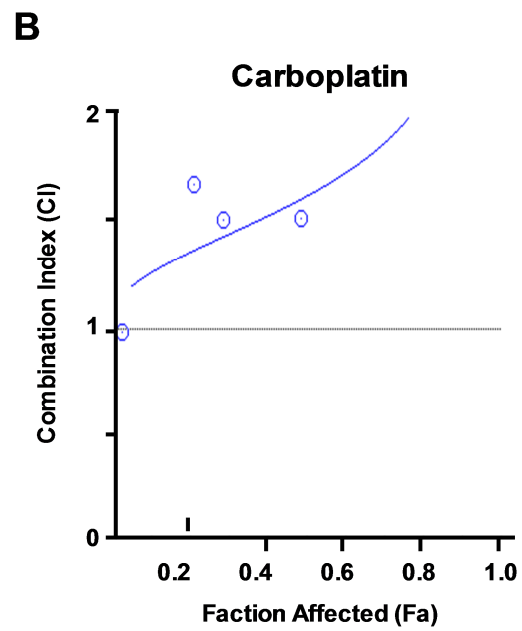
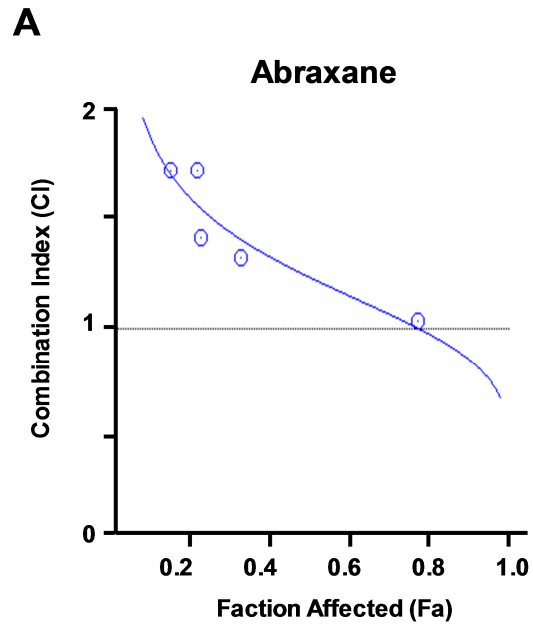
B



Supplemental Fig. S5. ADI-PEG20 induces mitochondrial fragmentation in MDA-MB-231 cells. (A) The mitochondrial fission was more noticeable after ADI-PEG20 treatment in MDA-MB-231 cells. Representative MitoTracker images (N = 4 sets of cells) with zoomed (*right*) are shown. (B) ADI-PEG20 increases lipid droplet accumulation. Representative transmission electron microscopy (TEM) micrographs from 10 images are shown. Boxed areas in *upper panels* are zoom images from below. Vehicle-treated MDA-MB-231 cells had normal mitochondria and intact cristae (*left panels*). A representative image shows a mitochondrion was wrapped with a double-membraned structure, as indicated by an arrow (*lower right panel*). An increase in the numbers of lipid droplets is also noticed. N: nucleus; M: mitochondria; LD: lipid droplet. Bar: 1 μm (*upper panels*) and 200 nm (*lower panels*); N = 3 sets of cells



Supplemental Fig. S6. ASS1 abundance predicts OS. (A) Multivariate Cox analysis shows reduced hazard ratio for overall survival of patients with high ASS1-abundance breast tumors. (B) Multivariate Cox analysis was used to adjust the hazard ratio for disease-free survival of patients with high ASS1-abundance breast tumors. Kaplan-Meier analysis determined the survival of subgroups of patients with high or low ASS1 abundance breast tumors that were ER negative (C), PR negative (D), Ki-67 positive (E), HER2 negative (F) and HER2 positive (G). Multivariate Cox analysis was applied to further determine the relative disease-specific death risk (hazard ratio) in the above subgroups. The ASS1 hazard ratios were based on high abundance versus low abundance. #: note that no hazard ratio is shown for patients who had breast cancers with high ASS1 abundance in the ER negative and HER2 positive subgroups because there were no breast cancer-associated deaths in those subgroups during the follow-up period. (H) Breast cancer specimens from patients with longer than five years of overall survival or disease-free survival have higher *ASS1* mRNA abundance. Analyses were performed using microarray-determined *ASS1* mRNA abundance and stratified with associated clinical data extracted from published NKI295 breast cancer data (57, 58) using shared software at ITTACA (<http://bioinfo-out.curie.fr/ittaca>). For Overall Survival, > 5 years: n = 231 and < 5 years: n = 61; for Disease-free Survival, > 5 years: n = 196 and < 5 years: n = 99; *: $p < 0.05$.



Supplemental Fig. S7. Lack of synergistic effect of ADI-PEG20 combined with Abraxane or carboplatin. The combination index for ADI-PEG20 and Abraxane (A) or carboplatin (B) was calculated as described in Fig. 6F.

Table S1. Primer sequences.

Name	Forward	Reverse
<i>ASS1</i>	5'-GAGGATGCCTGAATTCTACA-3'	5'-GTTGGTCACCTTCACAGG-3'
<i>SOD1</i>	5'-CGAGCAGAAGGAAAGTAATG-3'	5'-AGCAGGATAACAGATGAGT-3'
<i>SOD2</i>	5'-AGTTCAATGGTGGTGGTCATA-3'	5'-CAATCCCCAGCAGTGAATAA-3'
<i>SOD3</i>	5'-ACGCTGGCGAGGACGACCTG-3'	5'-GCTTCTTGCCTCTGAGTGCTC-3'
<i>SIRT1</i>	5'-TAGACACGCTGGAACAGGTTGC-3'	5'-CTCCTCGTACAGCTTCACAGTC-3'
<i>SIRT2</i>	5'-CTGCGGAACTTATTCTCCCAGAC-3'	5'-CCACCAAACAGATGACTCTGCG-3'
<i>SIRT3</i>	5'-CCCTGGAAACTACAAGCCCAAC-3'	5'-GCAGAGGCAAAGGTTCCATGAG-3'
<i>SIRT4</i>	5'-GTGGATGCTTTGCACACCAAGG-3'	5'-GGTTCAGGACTTGGAACGCTC-3'
<i>SIRT5</i>	5'-GTCCACACGAAACCAGATTTGCC-3'	5'-TCCTCTGAAGGTCGGAACACCA-3'
<i>SIRT6</i>	5'-TGGCAGTCTTCCAGTGTGGTGT-3'	5'-CGCTCTCAAAGGTGGTGTGAA-3'
<i>SIRT7</i>	5'-TGGAGTGTGGACACTGCTTCAG-3'	5'-CCGTCACAGTTCTGAGACACCA-3'
<i>GAPDH</i>	5'-CCCCTTCATTGACCTCAACTA-3'	5'-CTCCTGGAAGATGGTGTGG-3'
<i>18S</i>	5'-CGTCTGCCCTATCAACTTTCG-3'	5'-GGATGTGGTAGCCGTTTCTCAG-3'